Ocean Engineering 285 (2023) 115249

Contents lists available at ScienceDirect

Ocean Engineering

journal homepage: www.elsevier.com/locate/oceaneng

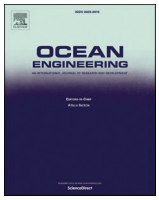

Development of a semi-empirical wake formation and dissipation prediction model for HAHT placed in channel flow

C.M. Niebuhr [a,*], M. van Dijk [a], L. Smith [b]

[a] Department of Civil Engineering, University of Pretoria, Pretoria, 0001, South Africa
[b] Department of Mechanical Engineering, University of Pretoria, Pretoria, 0001, South Africa

ARTICLE INFO

Handling Editor: Prof. A.I. Incecik

Keywords:
Hydrokinetic
Computational fluid dynamics
Wake prediction
In-land hydrokinetic
Axial flow turbines

ABSTRACT

Hydrokinetic (HK) energy production has been primarily developed for use in tidal energy applications. However, where inland water infrastructure systems with sufficient velocities and spatial requirements exist, HK energy may hold great potential. A first order estimate of the wake length and dissipation rate behind a device is necessary for installation design and analysis. Some analytical approximations have been developed to estimate the wake field, although the majority of these approximations do not consider operational conditions in confined flow settings. This paper focuses on the development of a new semi-empirical model for the prediction of the wake formation, dissipation, and flow recovery. Various HK turbines are modelled, and benchmark validated using commercially available computational fluid dynamics software. The developed semi-empirical wake model adequately predicts wake behaviour over a range of performance conditions (linked to the specific turbine thrust), ambient turbulence conditions as well as blockage ratios, which are all important parameters in inland flow applications. The model enables an approximation of the wake behaviour with an accuracy of within 10% over the tested range of turbines. This approximation is valuable for facilitating the planning of turbine placement and determining the spatial requirements for inland hydrokinetic (HK) schemes.

1. Introduction

Renewable energy technologies, such as small-scale hydropower systems, provide a clean energy source with a dependable base load. The climate crises and increasing electricity demand calls for new solutions and a need to capture “hidden” renewable energy sources. One example exists within hydrokinetic (HK) micro-hydro systems (Williams and Jain, 2011).

The kinetic energy in channels/canals with a sufficient flow velocity provides a predictable and extractable energy source (Guerra and Thomson, 2019). A HK turbine is designed to directly capture the kinetic energy of flowing water and generate electricity through thrust induced rotating blades. Although this type of hydropower does not necessitate civil works or modifications to water courses, the presence of the turbine leads to a disturbance that induces a pressure drop. Consequently, an axial pressure gradient is formed, giving rise to the formation of the wake (Sanderse et al., 2011). This wake is characterized by a significant velocity deficit and turbulent flow field (Lam et al., 2011). A comprehensive understanding of the hydrodynamics of these systems is crucial to ensure the safeguarding of watercourses and the surrounding areas. Additionally, it plays a vital role in turbine design and resource assessment (Guerra and Thomson, 2019), to harness this energy and allow a larger rollout of commercial HK devices. Accurate prediction of the wake length and dissipation rate is essential for optimising the energy extraction of turbine arrays (Chawdhary et al., 2017).

In recent years, several analytical and empirical approaches have been developed to allow simpler and faster approximations of the wake downstream of HK devices. Most have been developed for tidal applications (Ma et al., 2018; Pyakurel et al., 2017a) and thus unbounded flow. These analytical models are based on equations derived through the axial momentum theory, multiple stream tube theory and the lifting line theory. In the past, these were utilised for simplified performance analysis and have only recently been employed for wake characterization and turbine spacing (Lam and Chen, 2014).

A thorough understanding of the driving factors behind wake formation and dissipation is necessary to develop analytical wake models. The following factors have been considered in literature:

- Operational parameters such as tip speed ratio (λ) (Mourad et al., 2015) (Siddiqui et al., 2017) and turbine thrust have been linked to near wake formation.

* Corresponding author.
E-mail address: Chantel.niebuhr@up.ac.za (C.M. Niebuhr).

https://doi.org/10.1016/j.oceaneng.2023.115249
Received 29 March 2023; Received in revised form 19 June 2023; Accepted 24 June 2023
Available online 10 July 2023

Nomenclature

A	Area
AD	Actuator disk
b	Channel width
BEM	Blade element momentum
C	Empirical coefficient
CA	Channel aspect ratio
CFD	Computational fluid dynamics
D	Turbine diameter
dt	Rotor diameter length metric
Fr	Froude number
g	gravitational acceleration
HAHT	Horizontal axis hydrokinetic turbine
HK	Hydrokinetic
LPS2	Linear pressure strain 2-layer turbulence model
LR	Left rotor
$P_{position}$	Pressure
RANS	Reynolds averaged Navier Stokes
Re	Reynolds number
R	Rotor radius
rmse	Root mean square error
RR	Right rotor
RSM	Reynolds stress model
T	Thrust
TI	Turbulence intensity
TKE	Turbulent kinetic energy
U	Velocity
URANS	Unsteady Reynolds averaged Navier Stokes
VC	Volumetric control
VD	Virtual disk
V	Point velocity
V_x	Velocity deficit
W	Channel width
X	Position
β	Blockage ratio
λ	Tip speed ratio
ρ	Density

Subscripts

D	Drag
∞	Freestream
w	Wake
T	Thrust
P	Power
o	Available

- Additional parameters such a flow velocity, Reynolds number and additional blockage caused by turbine retaining structures or grids have been found to affect wake formation.
- It has been observed that ambient turbulence has a significant impact on the overall dissipation rate of the wake (experientially (Milne et al., 2013) (Lo Brutto et al., 2015) and numerically (Ahmadi, 2019) (Pyakurel et al., 2017b)).
- Blockage ratio (β) (Consul et al., 2013a; Koh and Ng, 2017) and depth below the free surface (Whelan et al., 2009) have been shown to influence turbine performance as well as wake dissipation rate and wake symmetry.

The consideration of these effects vary depending on specific installations, such as tidal or inland channels, where spatial constraints and array configurations differ.

The past studies mentioned are valuable for simplifying wake prediction. However, a simplified methodology for predicting wake lengths specifically for inland applications is currently unavailable. This paper aims to utilise a combination of literature findings and validated computational fluid dynamics (CFD) analyses to develop a new semi-empirical wake model. This model will be specifically designed to account for the typical installation conditions and turbine operating conditions in inland channels.

2. Background

2.1. Wake formation

Placing a turbine in a moving flow field causes a disturbance in the downstream region. This region is characterized by intense turbulent mixing, helical movements, and a complex eddy system, referred to as the wake. The wake characteristics may be attributed to two distinct phenomena. The first is the instability of the boundary layers on the blades caused by the adverse pressure gradient along the rotor plane. The second is the formation of a spiral vortex structure that emanates from the blade tip and rotor root, resulting in the generation of long-lasting large eddies in the downstream flow field (Silva et al., 2016) (as portrayed in Fig. 1).

The theoretical principles in Fig. 2 may be used to describe a turbine wake and propagation thereof. Consider a turbine of area A in a channel with cross sectional area A_c. Cross section A_o is the streamtube area of the upstream undisturbed flow, with the pressure p_o and flow speed u_o.

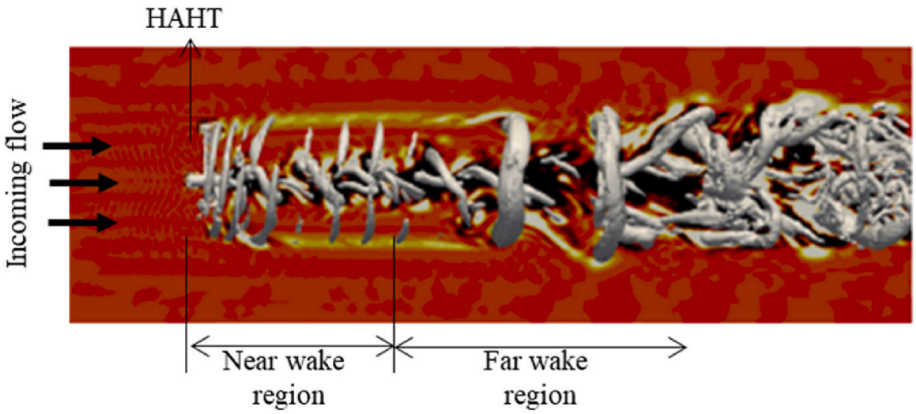

Fig. 1. HAHT wake (adapted from (Lloyd et al., 2014)).

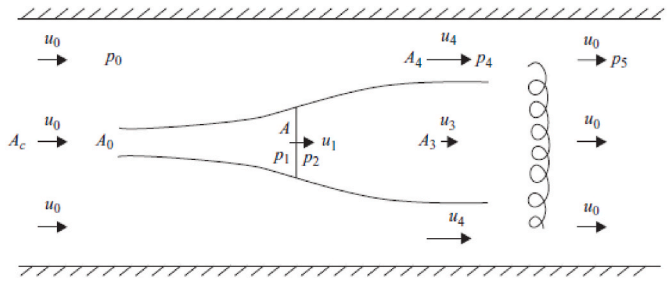

Fig. 2. Definition for single turbine in a channel (Garrett and Cummins, 2007).

The streamtube pressure is p_1 just upstream of the turbine and p_2 just downstream (assumed uniform as in the Lanchester-Betz formulation (Garrett and Cummins, 2007)). The streamtube expands downstream of the turbine and continues to do so before settling to a constant area A_3 with speed u_3. The flow speed outside the wake zone is defined by parameters u_4 and pressure p_4.

As portrayed on the sketch, when A_c approaches infinity, $p_4 = p_0$ and $u_4 = u_o$ (depending on the blockage ratio). The flow further downstream allows lateral mixing, resulting in a pressure change to p_5, which varies from p_0. The equation for energy extraction is derived (Garrett and Cummins, 2007) by applying the conservation momentum and conservation of energy to the above mentioned flow. In a channel with an infinitely large domain the maximum efficiency for power extraction has been determined to be approximately 59% commonly known as the Betz limit. Nevertheless, the impact of confinement on this efficiency has not been extensively studied, and it has been observed to surpass this limit (Cardona-Mancilla et al., 2018).

In the immediate downstream region of the turbine, the wake physics becomes complex and is influenced by various factors, including the bypass flow, induced flow from the rotor and the interaction of specific tip vortices with the supporting structure (Olczak et al., 2016). Further downstream the wake begins to mix with the bypass flow, leading to the expansion of the wake and gradual recovery of velocity over an extended distance. This defines the two predominant behaviours and regions which are more generally referred to as the near wake and far wake. The near wake may be characterized as a connected structure associated with vortex shedding behaviour. The far wake is associated with global instabilities and inhibits a slow movement of the whole mean velocity field. The near wake is specifically characterised and affected by the turbine geometry, whilst the far wake is not (Lam and Chen, 2014). The presence of tip vortices is clearly seen in this region. The formed tip and root vortices result in sharp velocity gradients and peaks in turbulence intensity. For extremely high tip speed ratio's, a vortex street may form downstream as the tip vortices join, forming a shear layer (Sanderse et al., 2011) and slower rotations. As a result, this process exhibits a behaviour similar to that of the Karman vortex street (Tian et al., 2018).

In the far-wake region, turbulence intensifies and the interaction between the bypass flow and wake flow regions become more stochastic, leading to increased mixing. Two primary features exist in the wake, low water speeds and a high turbulence intensity (Ge et al., 2019), the former of which reduces the power output of any subsequent turbine in its wake.

2.2. Factors affecting wake formation and recovery

The wake behaviour of a turbine is influenced by several physical processes present in the flow. These include the onset shear and turbulence, interaction with retaining structures, tip vortices, and wake rotation (as indicated in Fig. 3). However, there have been limited studies that have extensively investigated the impact of these factors on the far wake.

The inlet/ambient turbulence intensity (TI) acts as an effective mixer. This leads to wake recovery and thus a decrease in overall turbulence intensity. TI is the primary driver to wake dissipation and recovery. Multiple studies have investigated the effect of wake dissipation and wake extents at different levels of ambient TI (Lo Brutto et al., 2015; Pyakurel et al., 2017b; Birjandi et al., 2012; Mycek et al., 2014). These studies found that as turbulence levels were increased, the wake dissipation rate increased, reaching lower velocity deficits closer to the turbine. It was also found that wake expansion increased closer to the turbine at higher TI levels (Lo Brutto et al., 2015) (Pyakurel et al., 2017c). Maganga et al. (2010) tested the effect of ambient TI on the wake for a 3-bladed horizontal axis turbine at $\lambda = 9$, placed in two different ambient turbulence scenarios namely 8% and 25%. Wake comparison indicated a maximum recovery of close to 60% by 4.4 d_t (diameter downstream) for a TI = 8%, and 60% by 1.4 d_t downstream for a TI = 25%. Similarly, an 80% recovery in streamwise velocity was found at 9 d_t for a test case with onset TI = 8% and 3 d_t for onset TI = 25%.

Blockage ratio (β) has been shown to significantly alter turbine performance at ratios exceeding 5–10% (Kolekar and Banerjee, 2015). Generally for turbines operating at a given tip speed ratio, higher β results in an increased streamwise flow speed through and around the rotor which in turn increases the turbine torque and thrust (Ross and Polagye, 2020). Details of the effects on turbine hydrodynamics are given in (Houlsby et al., 2017; Consul et al., 2013b). Significant increases is C_P and C_T have also been attributed to the acceleration of the bypass flow (Nishino and Willden, 2012). A major challenge exists in experimental validation of β effects, encompassing both turbine behaviour and multiple analytical corrections. This is due to the difficulty in conducting experiments requiring varying β's whilst controlling

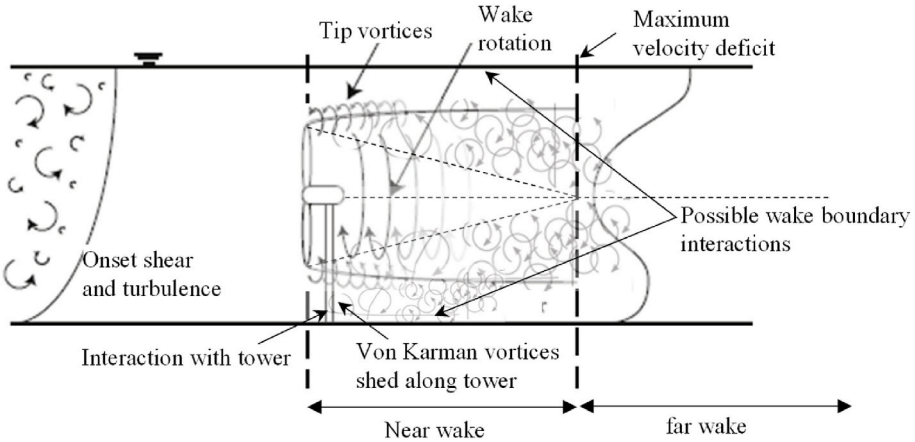

Fig. 3. Schematic of flow affecting the loading and wake of a HK device (adapted from (Niebuhr et al., 2022)).

Reynolds dependence and considering the effects of the free surface (submergence depth) and Froude number (Fr) (Ross and Polagye, 2020). An example of the β effect on the power and thrust curves for axial turbines can be seen in Fig. 4. Past studies have also reported the insensitivity of C_p to β at low λ's (Kolekar et al., 2013) (Kinsey and Dumas, 2017). Generally, turbines perform better at higher blockage coefficients, but this has a limit.

The effect of the depth the HK device is placed below the free surface may influence turbine performance as well as wake recovery. Complexities arise when turbines are placed near the free-surface, as the boundary may modify the turbine flow-field and affect device performance. In general, this causes significant flow acceleration, with the magnitude of acceleration depending on the blockage ratio. Kolekar and Banerjee (2015) found that there exists an optimal clearance depth (depth from blade tip to free surface) resulting in improved turbine performance, which should be considered during relevant installations.

The shape and size of the retaining structure as well as a grid or any other element placed in the flow field may affect the wake propagation downstream. Even more so in inland HK applications where blockage ratios are high. Many studies have concluded that turbine geometry may affect the shape of the near wake but have negligible effect on the far wake (Lam and Chen, 2014). Siddiqui et al. (2017) found a faster recovery rate due to the presence of a turbine tower. Zhang et al. (2020) investigated the wake of a horizontal axis tidal stream turbine supported by a monopile and found that the monopile strongly affects the flow field within three rotor diameters downstream, this resulted in an asymmetric recovery trend for the velocity. An interesting finding noted the high disturbance in the near wake of a HK device due to the turbine hub, body and support structure at a low ambient TI (TI = 8%) which was not noticeable at a high ambient TI case (TI = 25%). This phenomenon can be attributed to the faster decrease in velocity deficit and the subsequent absence of wake development caused by the hub. The vertical structure of the wake is also more prevalent at lower TI's (Maganga et al., 2010).

A summary of the factors found to affect wake recovery, as well as references to literature investigating these effects can be seen in Table 1.

Table 1
Factors investigated for wake effects.

	Quantified significant effect on the wake	Quantified insignificant effect on the wake	Investigation and unquantified effect on the wake
Free stream turbulence	(Lo Brutto et al., 2015) (Pyakurel et al., 2017b) (Birjandi et al., 2012) (Mycek et al., 2014) (Pyakurel et al., 2017c) (Blackmore et al., 2014)		Maganga et al. (2010)
Depth below free surface	Silva et al. (2016)	(El Fajri et al., 2020) (Myers and Bahaj, 2007) 13]	Stallard et al. (2013)
Blockage ratio	Stallard et al. (2013).		(Stallard et al., 2013) (Nishino and Willden, 2012)
Turbine geometry/ retaining structure			Lam and Chen (2014)
Debris protection grids	-	-	-
Turbine operational conditions (thrust/λ)	(Wang et al., 2018) (Tian et al., 2018) (Harrison et al., 2010)		
Turbine array effect	(Stallard et al., 2013) (Macleod et al., 2002) (Stallard et al., 2013)		(Churchfield et al., 2013) (Gotelli et al., 2019)
Reynolds number			Bachant and Wosnik (2016)

2.3. Existing wake models

Studies have demonstrated that HK wakes result in downstream velocity deficits ranging from 10 to 20 rotor diameters downstream (Mycek et al., 2014) (Maganga et al., 2010). Therefore, quantifying the dissipation rate of turbine wakes is crucial for conducting performance and placement analyses of turbine arrays (Pyakurel et al., 2017c).

Previously, analytical wake prediction models have been developed through various approaches. These have been developed based on the axial momentum theory, actuator disk model (CFD approach) and empirical relationships through experimental work. Lam & Chen (Lam and Chen, 2014) proposed a set of equations to predict the lowest velocity closest to the turbine, which were derived from the axial momentum theory combined with a dimensional analysis. The term efflux velocity is used to define the minimum velocity taken from a time-averaged velocity distribution along the initial turbine plane. This is also the point of lowest velocity in the wake (maximum velocity deficit) and the point where wake recovery starts. For Lam & Chen's model the efflux velocity is used in a defined equation to calculate the minimum velocities at respective points downstream. The efflux velocity was derived as a function of the free stream velocity based on the propeller jet theory.

Wang et al. (2018) noted the importance of considering turbine solidity and λ when calculating the efflux velocity and adapted the Lam & Chen model to include an additional term E, which is a function of λ. Lam et al. (2015a) noted the strong effect of TI on the wake and therefore suggested a separate set of equations for low TI (3%) and high TI (14%) cases, based on the distance from the hub.

Several analytical wake models have previously been used to model the wake behind a wind turbine, such as the Jensen (1983), Larsen (1988) and Frandsen (Frandsen et al., 2006) model's. Pyakurel et al.

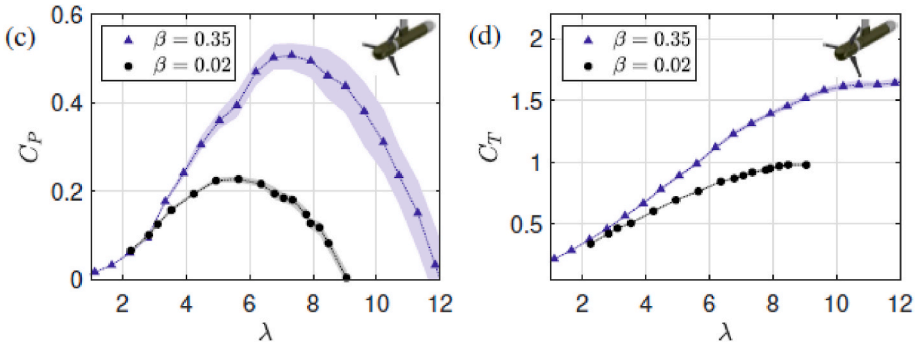

Fig. 4. Confined and unconfined power and thrust coefficient for axial flow turbines (shading represents uncertainty) (Ross and Polagye, 2020).

(2017a) developed an analytical HK wake prediction model based on three wind turbine models (Larsen, Jensen and Ainslie approach) and adjusted the models to account for ambient turbulence. CFD analyses were used to optimize the coefficients α (Jensen model) and c_1 (Larsen model). The model was developed for tidal installations with no blockage ratio incorporated due to the lack of experimental data (Pyakurel et al., 2017c). The study found the Larsen model exhibited superior performance for ambient turbulence intensities (TI) of 3%, whilst the Jensen model was more suitable for TI values of 6% and 9%. Although both models did not show good correlation to CFD results.

Lo Brutto et al. (2015) used an adaptation of the Jensen model to calculate the axial velocity profiles in the wake of turbines with small diameter to depth ratios (20%). Their work aimed to improve the work by Palm et al., 2010, 2011 by taking into account the thrust coefficient (C_T) and the ambient turbulence in comparison to CFD data. Using these equations, it was possible to estimate the velocity in the wake of the turbine for difference values of ambient turbulence (I_0).

While the previously developed wake models might have been designed for different applications, such as wind turbines, or may require additional validation, their initial development and the factors considered can still provide insight into the variables that have the most significant impact on wake development and recovery. This information can be valuable in assessing and understanding wake characteristics across different turbine geometries and applications. A summary of wake models which have been considered or developed for HK turbines as well as the variables considered in each model are listed in Table 2.

Whilst each model mentioned in Table 2 is valuable for open flow applications, they provide inadequate results for inland HK turbines operating in bounded flow conditions. This inadequacy results from the models lack of inclusion of consideration for blockage (in all models) and ambient turbulence (in most models). The objective of this study is to address these limitations by incorporating the necessary variables and advancing the development of analytical models. This was achieved by collecting a more extensive dataset of wake formations and building upon the prior research mentioned in Table 2.

3. Method

A semi-empirical approach was employed in this study, wherein fundamental hydrodynamic laws were utilised to derive basic equations. Metrics found to significantly alter the wake formation and dissipation were included empirically. These equations were then employed to develop a simplified wake model.

3.1. Semi-empirical wake model development

The solution objective of the wake model is to determine the wake recovery over a diametrically proportional distance downstream of the turbine blades ($x/D = d_t$) averaged over an area equivalent to the swept area of the blades (A_D) as shown in Fig. 5. This particular quantification was chosen because the primary objective of the model is to determine the inlet velocity of a downstream turbine. The asymmetric nature of the wake is evident in Fig. 5 and the averaged value over the area is indicated, projected over the swept area.

To simplify the wake model, the wake is characterized into 3 properties as seen in Fig. 6:

1. The minimum velocity point (averaged over the turbine swept area) $V_{OD.}$
2. The point at which this low velocity zone occurs ($X_{\min}$).
3. The dissipation rate after V_{OD}.

3.2. Collection of wake data

A limitation in the development of analytical models is the availability of a reliable wake dataset. CFD modelling was used to generate a significant dataset on a range of turbine types and operational conditions. A rigorous validation procedure was completed to ensure a reliable dataset.

Siemens STAR-CCM + software was used to model wall bounded three-dimensional models at full scale. Firstly, replications of the benchmark validation cases were modelled for verification of the CFD approach, after which input parameters were varied to create a larger dataset. Careful selection of flow physics, and comparisons of commonly used models is a crucial factor in accurate modelling of these complex flow fields. A Reynolds averaged Navier Stokes (RANS) approach was selected due to the reduced computational demand. A Reynolds stress model (RSM), specifically the Linear pressure strain 2-layer (LPS2) turbulence model, was employed, as this proved to best replicate experimental results. Transient simulations were performed for all models where unsteady terms were discretised using a 2nd order implicit scheme. The upstream boundary was specified as a velocity inlet, with a constant velocity distribution. The model was found to perform best when the boundary layers were allowed to form freely (by extending the inlet length) based on the non-slip wall condition specified. A pressure outlet was used to simulate the model outflow conditions with an environmental condition specified (to prevent backflow). Full development of the boundary layer on all surfaces was ensured through the specific turbulence model wall treatment and mesh resolution for each test case.

A virtual disk (VD) was used to represent the rotor, and a blade element momentum (BEM) model was employed. A BEM tip-loss correction was incorporated using the Prandtl tip loss correction method (Shen et al., 2005). The virtual disk required rotor geometry and aerodynamics performance metrics (lift and drag coefficients). The rotor geometry metrics in terms of chord length, twist, pitch and number of blades was included in the model. Lift and drag coefficients (C_L and C_D) generated in XFOIL software as well as past experimental results on the blade profile over a range of Re's ($200\,000 < \mathrm{Re} < 3\,000\,000$) were added to the VD-BEM model. A detailed description of the CFD approach

Table 2
Wake models and factors considered in each model.

Model	Governing equation	Considered variables f{}
Larsen, 1988 (Larsen, 1988)	$U_c = 1 - \frac{V_x}{U_o} = \frac{1}{9}(C_T A_d x^{-2})\frac{1}{3}\left(\left(\frac{35}{2\pi}\right)^{\frac{3}{10}}(3{c_1}^2)^{\frac{-1}{5}}\right)^2$	Downstream velocity (V_x), Thrust coefficient (C_T), non-dimensional mixing length (c_1) Rotor diameter (A_d)
Jensen, 1983 (wind turbine model) (Jensen, 1983)	$V_x = U_o\left(1 - 2a\left(\frac{R}{R+\alpha x}\right)^2\right)\ a = 1 - \sqrt{\frac{1-C_T}{2}}$	Free stream velocity (Uo), empirical coefficient (α), axial induction factor (a) (in terms of C_T) and Rotor radius (R)
Lam and Chen. 2015 (Lam et al., 2015b)	$V_{min} = \left(0.0927\left(\frac{x}{D}\right) + 0.993\right) \times V_\infty\sqrt{1-C_T}$	Free stream velocity (V_∞), thrust coefficient (C_T)
Pyakurel et al., 2017 (Adapted Jensen and Larson coefficients) (Pyakurel et al., 2017a)	$\alpha = 0.00003TI^4 - 0.0009TI^3 + 0.0097TI^2 - 0.0396TI + 0.0763\ c_1 = 0.0406e^{0.1361TI}$	Turbulence intensity (TI)
Oppong et al., 2020 (Oppong et al., 2020)	$V_o = \sqrt{(V_\infty)^2 - (1.59(n_o - n)D\sqrt{C_T})^2}$	Free stream velocity (V_∞), thrust coefficient (C_T), rotation rate (n) and turbine diameter (D)

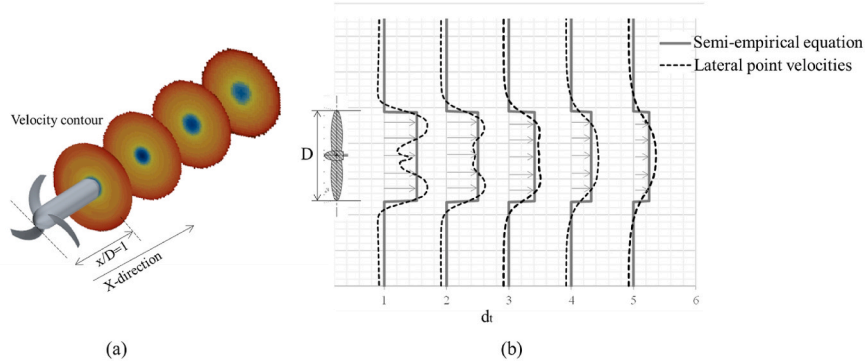

Fig. 5. Wake model diagram (a) velocity map over swept area (b) averaged wake deficit values vs true lateral wake measurements.

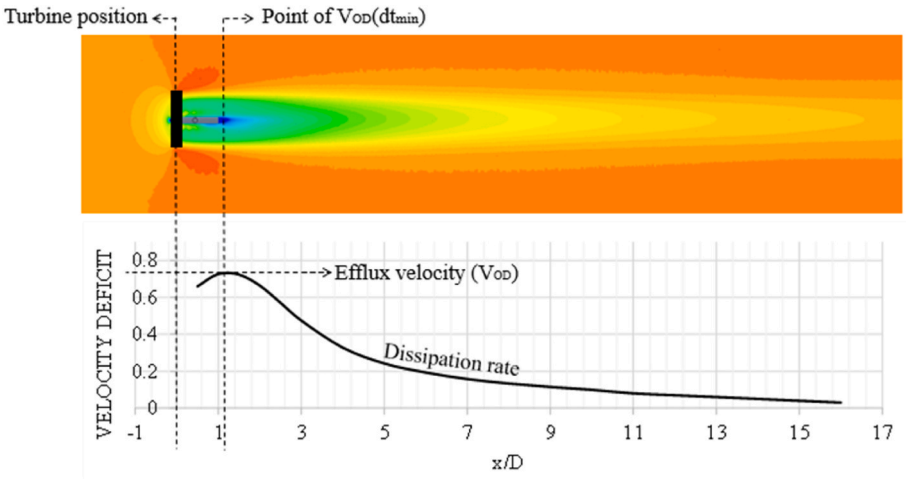

Fig. 6. Wake model parameters.

used can be seen in previous work (Niebuhr et al., 2022).

Six HK turbines with existing laboratory or experimental wake and/or performance results were used as benchmark validation cases. CFD models using a RANS-Reynolds stress approaches were simulated (see full method in (Niebuhr et al., 2022)):

- **T1 model:** The RM1 2-bladed (Hill et al., 2014, 2020) laboratory test turbines were modelled in CFD. Benchmark validation of wake dissipation was done through a comparison of wake velocity and turbulence profiles (d_t = 1–22). Power output and performance metrics were also compared (see (Niebuhr et al., 2022)).
- **T2 model:** The IFREMER-LOMC 3-bladed (Mycek et al., 2014) turbine laboratory setup was modelled. Benchmark validation was completed through wake velocity contour comparisons (d_t = 1–10), power output (W) comparisons and C_P and C_T results.
- The 2, 3 and 4-bladed 0.5 m diameter turbines built and tested at Liverpool University (Morris, 2014; El Fajri et al., 2022; Tedds et al., 2014; Morris et al., 2016) (**T3 model**) as well as a 3-bladed BBMC 0.8 m diameter turbine (Bahaj and WMJJMcCann, 2007) (**T4 model**) were modelled. C_p and C_T results were used to validate the model applicability.

An example of the modelling approach and mesh can be seen in Figs. 7 and 8. A virtual disk (VD) was used to model the turbine rotor. The experimental performance results (Fig. 9b) indicated that the virtual disk model adequately captured the turbine performance and validated the correctness of the parameters incorporated in the virtual disk model.

For computational models, it is crucial to conduct a mesh-independent study and utilise a validated mesh to ensure appropriate

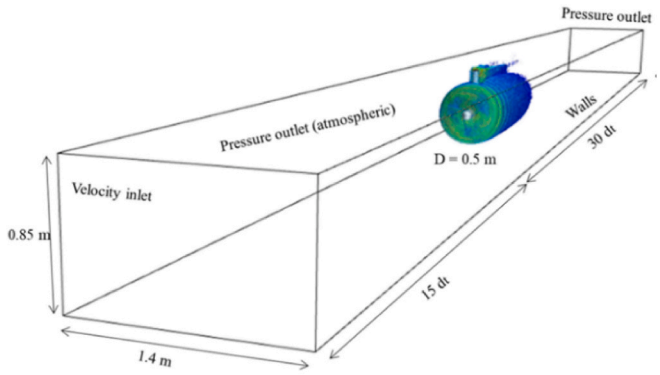

Fig. 7. T3 turbine model domain.

solutions across all parameters. The correct grid refinement rules were determined through a grid convergence test process. A polyhedral mesh with volumetric refinements in the near and far wake was used to ensure the wake effects were captured. Surrounding the VD, a local mesh refinement of 0.8% of the turbine diameter was found to adequately capture performance. This is true for λ's up to 5.1, higher values could possibly require smaller grid refinements due to changes in local courant numbers. For proper formation of the near wake a mesh size of 1.5% of the turbine diameter was necessary. A minimum mesh of 2.5% of the diameter provided an accuracy of within 5% of experimental wake dissipation rates up to 6 d_t downstream. After 10 d_t the dissipation rate was predicted within 1% accuracy for the courser mesh as the near wake

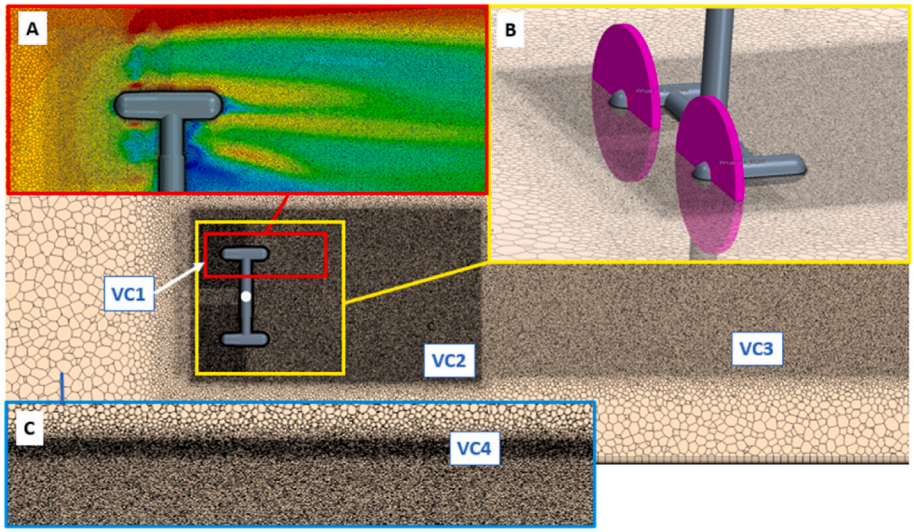

Fig. 8. BEM-VD model mesh with A- Refinement regions around the VD, B- VD placement and refinements and C- Free surface refinements (for multiphase models).

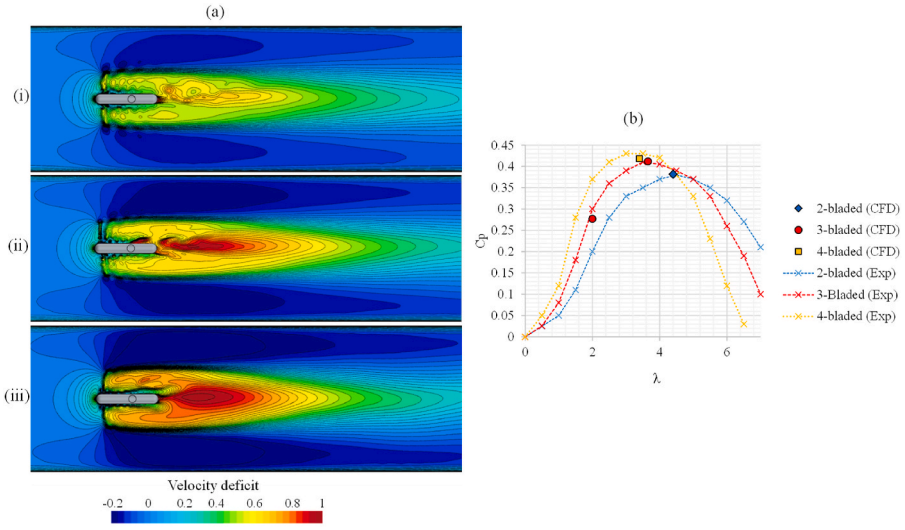

Fig. 9. T3 model turbine model (a) (i) 2-bladed (ii) 3-bladed and (iii) 4-bladed velocity contour and (b) performance comparison to experiment results.

effects became less prevalent. The flow field and far wake should be a maximum of 1.3% of the turbine diameter (as found for the IFREMER 15% TI case) to ensure correct incorporation of ambient turbulence (especially for higher TI values). Final mesh sizes of around 15 million cells were used in a transient analysis.

In summary, the primary flow conditions found to be most common to inland HAHT conditions and thus included in the verified models are shown in Table 3. The computation models were kept within these constraints.

Table 3
Range of inland flow conditions for HAHT application verified and validated by experimental results.

Variable	Range of values considered in the study	
	Min value	Max value
Flow velocity (U_∞)	0.8 m/s	3 m/s
Turbulence intensity (TI)	5%	20%
Froude number (Fr)	0.1	0.6
Channel flow Reynolds number ($Re_{channel}$)	300 000	900 000
Radius based Reynolds number (Re_D)	140 000	680 000
Blockage ratio (β)	5%	25%
Turbine diameter (Ø)	0.5 m	1 m

3.3. Metrics of consideration

As mentioned in section 2.2, multiple factors around the turbine operating conditions and environment affect the wake formation and dissipation. Many of these potential factors were varied over the CFD test cases to see which most affected the wake formation and should therefore be included in the model.

HAHT units are typically designed for specific operational conditions best suited for the turbine and retrofitted to a site. Although in some cases the applied resistance from the generator (torque) may be altered to suit the operational conditions, the turbine is usually provided with a set control system (maximum power point tracker) and pre-determined power curve (Niebuhr et al., 2019). Therefore, the turbine may operate at slightly higher or lower λ′s than the optimal conditions. Due to flow separation, self-starting abilities, as well as defined optimal operational conditions of previously tested turbines, the λ may be limited to a typical range of between 3 and 6.

Turbine thrust, and subsequent thrust coefficient, were found to be a

useful metric to measure the overall initial disturbance in the flow field. As mentioned, the optimum design, or selected turbine, may depend on supplier preference or availability. However, as the number of blades increases, the optimum λ decreases. This is also seen when comparing the C_p curves of a 2, 3 and 4-bladed turbine shown in Fig. 10. The optimum λ is typically consistent over a range of inlet conditions. The results from the 2-bladed NACA 4415 HAHT curves showed the left rotor (LR) and right rotor (RR) performed differently, however the λ for optimal performance is still consistent. A similar trend was observed throughout literature.

Similar to literature results (Kolekar and Banerjee, 2015) in this study the blockage ratio (β) was found to significantly alter the turbine performance at ratios exceeding 5–10%. The β is calculated as $\beta = (A_D + A_S)/A_C$ where A_S is the projected area of the support structure and A_C the projected area of the channel cross section perpendicular to the flow direction. During initial testing the blockage ratio was found to have a significant influence on the minimum velocity in the wake (V_{OD}) and thus also on the subsequent dissipation rate. The performance measurements also indicated that a significantly higher power output is achieved at higher blockage ratios, which also aligns with literature findings. For the case shown in Fig. 11 a C_P of 15% was obtained for a β of 7% case, compared to $C_P = 0.26$ in the 16% β case.

The effect of blockage ratio seems to lower the dissipation rate, but does not alter the dissipation relative to the minimum velocity point (V_{OD}), this can be observed through the normalized velocity deficit (*Velocity deficit*$/V_{OD}$) shown in Fig. 11. The clearest observed of this phenomenon is evident in the T3 results, although a similar result is also exhibited by the results of the other three turbines tested. Therefore, it can be concluded that β primarily affects the V_{OD} value and the dissipation behaviour is altered proportionally.

At extremely high blockage ratios ($\beta > 20\%$) the wake dissipation rate is accelerated by the blockage effect and the channel wall boundary layers. Although at lower β′s the effect of a higher bypass flow slightly increases wake dissipation, the effect is small. A comparison of the same 3-bladed turbine in a multiphase BEM-CFD analysis in a β of 23% vs β of 5% flow field can be seen in Fig. 12. The effects of the free surface as well as wall boundaries are prevalent. The free surface plays a larger role in the presence of a support structure as was shown by El Fajri et al. (El Fajri et al., 2020). The blockage in Fig. 12 resulted in a normalized velocity deficit differential of around 20%, compared to almost no differential at lower β′s as those included in Fig. 11. The gives an indication of more extreme wake dissipations in cases of $\beta \gg 20\%$. As turbine placement depths are usually limited by manufacturers the effect of near free surface turbines and higher β′s (β > 16%) was not considered in this study, however this should be considered in a future study and the model adapted accordingly.

The analysis included channel aspect ratios ($CA = W/H$ with $W =$ Channel width and $H =$ Channel height) of a CA of 0,5 to 1. Most analysis were in the range of $CH = 0.6$ to 0.7. Only smaller differences were attributed to aspect ratio variations, and therefore assumed negligible in this case. Future studies on a larger variation of aspect ratios would prove beneficial to validate this result. Further conclusions on aspect ratios were limited due to the scope limitation of available laboratory test results.

Higher turbulence intensities (TI) in a channel result in accelerated wake dissipation. The overall V_{OD} is decreased as the strong vortex structure is not allowed to form, and the position of the highest V_{OD} ($X_{\min}$) is decreased (the position of $X_{\min}$ moves closer to the turbine).

Streamwise turbulence intensity is commonly employed as a measure of turbulence in a channel or river section. Transverse and vertical intensities usually exhibit different ratios (Milne et al., 2013), with streamwise turbulence often being significantly greater in magnitude. Turbulence intensities in a smooth river or canal section are usually between 5 and 20%. Li et al. (2010) reported turbulence intensities of 25–30% in shallow water in the East River, New York (where $U_\infty = 2$ m/s).

In flow regions with higher TI's a reduction of $X_{\min}$ is commonly observed, where the occurrence of V_{OD} moves closer to the turbine due to accelerated wake formation and dissipation. The wake model was adjusted to account for typical behaviour observed in inland water reticulation systems, where the TI ranges from 5% to 20%. Although higher TI's may exist, they often lead to unfavourable installation conditions, and as a result, they were not included in the study. Although numerous previous studies have explored the impact of TI on wake formation, there have been relatively few analyses conducted on the far field characteristics of wakes. To ensure accurate capture of these effects, CFD tests were conducted across a range of TI values. This was done to generate a comprehensive dataset that could be utilised for the development of the semi-empirical wake model.

In summary, the primary factors considered to govern the wake formation and dissipation in the flow field of a HK turbine were: turbine thrust, which accounts for the operational λ and blade profile; The blockage ratio (β) which affects the power output and therefore also the maximum V_{OD} in the wake; as well as dissipation rate, which is accelerated at higher blockage ratios due to the confined bypass flow; And lastly the turbulence intensity (TI) in the flow field, which significantly accelerated the wake recovery at higher TI values. These metrics were included in each property as shown in Table 4.

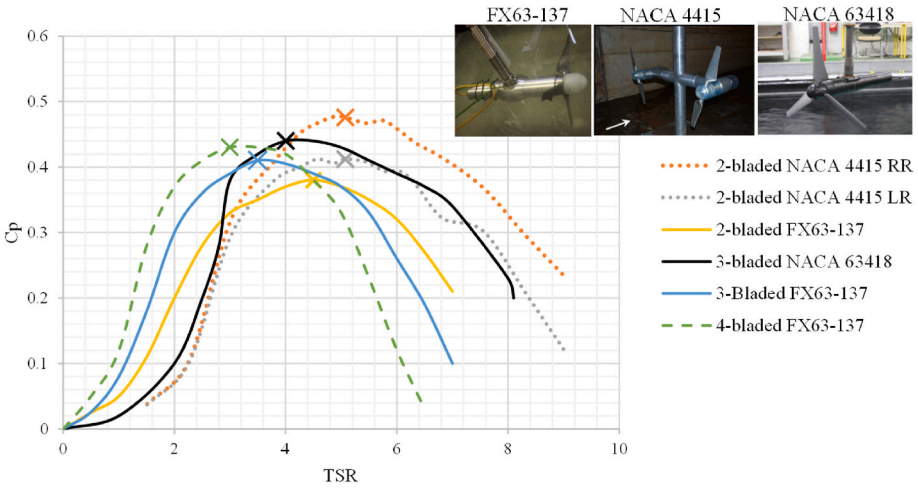

Fig. 10. Turbine performance comparison between the measured experimental results of the HAHT with NACA4415 (Hill and Neary, 2014), NACA 63418 (Mycek et al., 2014) and FX63-137 (Morris, 2014) blade profiles.

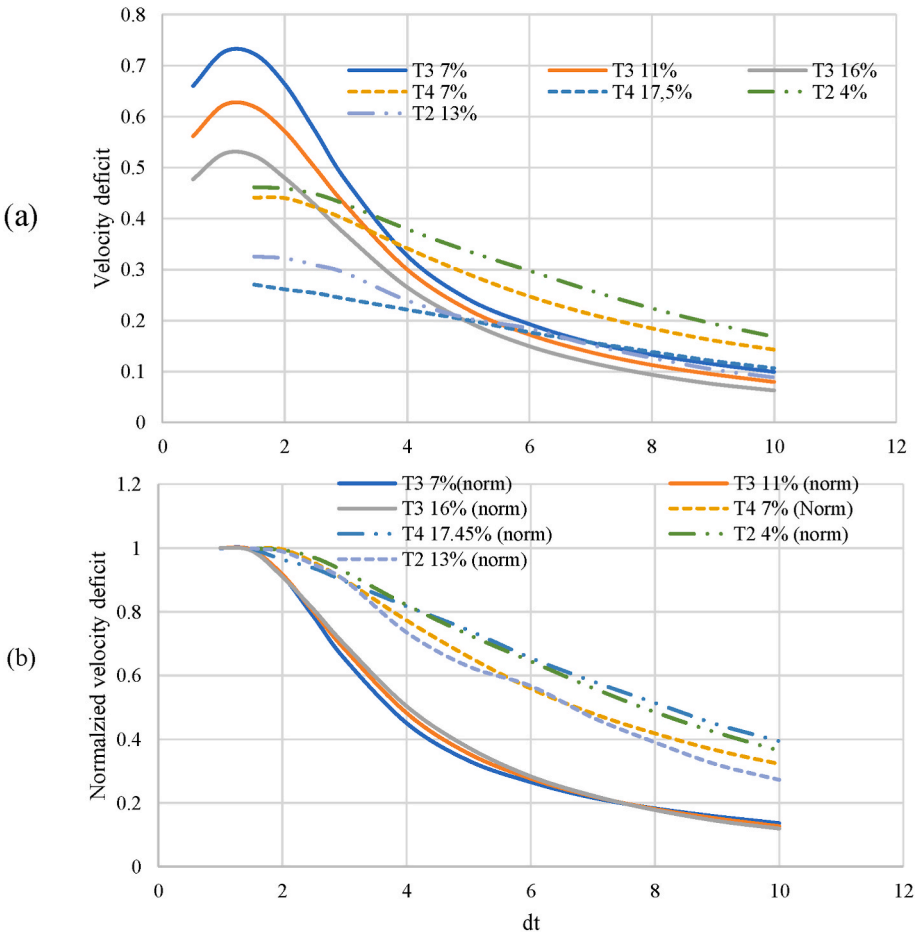

Fig. 11. Effect of blockage ratio (at 7%, 11% and 16%) on dissipation rate comparing (a) Velocity deficit and (b) normalized velocity deficit.

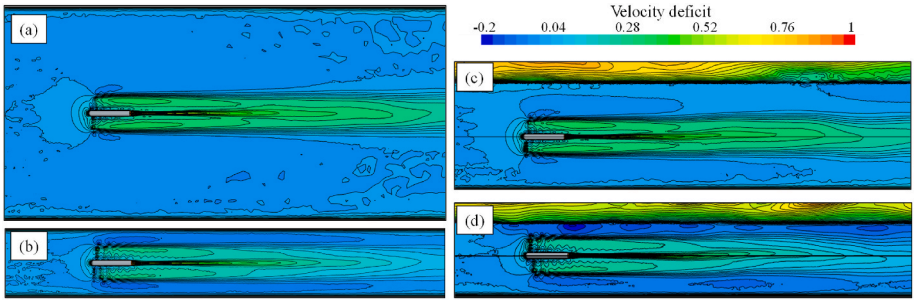

Fig. 12. Velocity deficit distribution surrounding a 3-bladed HAHT for a $\beta = 5\%$ (a) horizontal and (c) vertical profiles; a $\beta = 23\%$ (b) horizontal and (d) vertical profiles.

Table 4
Model considerations.

Property	Variable	Metrics of consideration
Minimum velocity point (over A)	V_{OD}	C_T, β, TI
Point at which minimum velocity occurs	$X_{\min}$	V_{OD}, TI
Dissipation rate (at points d_t downstream)	V_x ($d_t = x/d$)	V_{OD}, TI, β

3.4. Determination of minimum velocity in the wake (V_{OD})

A simple approximation for the minimum velocity just downstream of a HAHT is possible through the actuator disk theory. Fig. 13 shows the

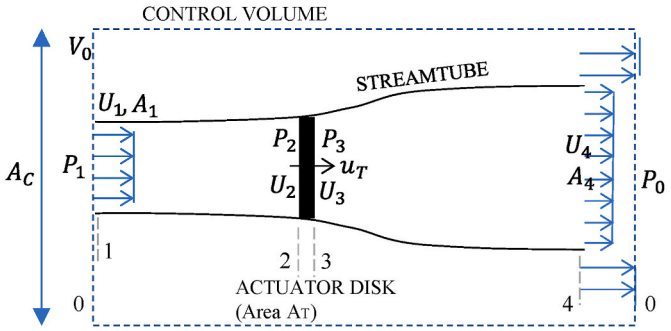

Fig. 13. Actuator disk model.

application of the axial momentum theory using an actuator disk principle, often used in wind turbine analysis (Eggleston and Stoddard, 1987). Applying the conservation of energy over this disk allows approximation of the minimum velocity downstream of the disk.

Assuming a very flat slope (thus ignoring the reference to a datum height) the energy upstream of the disk can be described with P_1, P_2, P_3 and P_4 are the pressures at points 1,2,3 and 4 (Fig. 13) and U_1, U_2, U_2 and U_4 the relevant velocities (m/s), ρ the density of water and g the gravitational acceleration.

As continuity must hold within the streamtube we know that:

$$U_1 A_1 = u_T A_T = U_4 A_4 \tag{1}$$

We also know that continuity holds over the control volume (upstream and downstream) and a net flow exists:

$$\Delta Q = V_0[(A_c - A_1) - (A_c - A_4)] = V_0(A_4 - A_1) \tag{2}$$

To quantify the change in momentum over the disk the effect of the disk can be simply expressed as a thrust (T) which is essentially the force (F) on the disk. To slow the water the force can be written as a static pressure drop over the disk, similar to the actuator disk approach, (assuming no periodicity or pressure variation with time).

Assuming the far upstream and far downstream pressure (P_1 and P_4) are equal and assuming the velocities directly upstream and downstream of the disks remain the same ($U_2 = U_3$). The Bernoulli energy equation can be combined with the thrust approximation and the following relationship is obtained:

$$T = \frac{1}{2}\rho A\left({U_1}^2 - {U_4}^2\right) \tag{3}$$

From the propeller jet theory it is known that axial thrust is produced through shaft torque by increasing the rearward momentum of the surrounding fluid (Stewart, 1992). This induces a reactive forward force from the fluid on the propeller (used for propulsion). By representing the propeller as an actuator disk consisting of an infinite number of rotating blades and assuming energy is supplied to the system as water passes through the jet. The change of momentum due to the energy supplied results in a net thrust on the fluid. Dimensional analysis of the propeller thrust allows the following relationship.

$$T = C_T \rho n^2 D^4 \tag{4}$$

Where n is the propeller rotation rate (rev/s), C_T the propeller thrust coefficient and D the propeller diameter. Combining this equation with equation (3) the minimum velocity in the wake (U_4) can be expressed as:

$$U_4 = \sqrt{{U_1}^2 - \frac{2C_T n^2 D^4}{A}} \tag{5}$$

However, this relationship does not translate well to turbines, as ship propellers typically operate at exponentially higher rotation rates compared to HK turbines in channel flows. As a result, an alternative definition for the thrust coefficient is employed. This approximation is commonly used to define the thrust of a wind turbine (Eggleston and Stoddard, 1987) and is described as the non-dimensional ratio of axial force to incoming flow momentum with U_∞ representing the freestream velocity:

$$C_T = \frac{T}{\frac{1}{2}\rho {U_\infty}^2 A_D} \tag{6}$$

By considering U_∞ equal to U_1 and combining equations (3) and (6) the following relationship for U_4 is determined, which would refer to the minimum velocity in the wake:

$$U_4 = \sqrt{{U_\infty}^2(1 - C_T)} \tag{7}$$

This minimum velocity in the wake (U_4) is often referred to as the efflux velocity (Lam et al., 2015a). As mentioned, in the current study it was found that the average velocity over the cylindrical area (V_{OD}) is most useful when determining turbine spacing (average velocity over disk area) which is, according to the equation derivation, equivalent to U_4, being an expression of the average velocity downstream of the disk (over the propeller swept area). Although this equation is useful in determining the minimum velocity in the wake based on the turbine C_T and flow velocity, it does not include any effects of ambient TI or blockage (β) which have been proven to affect the minimum velocity.

The β influences the turbine thrust and could therefore account for variations in the maximum V_{OD} in the wake. Previous studies have been conducted to explore blockage correction methods that account for laboratory test results for higher β's. These approaches are based on a concept introduced by (Glauert, 1983) for performance change effects in wind turbine wind tunnel testing. Typically, the model adapts the thrust coefficient approximation (equation (6)) with a new predicted freestream velocity (U_∞') which would, in unconfined conditions, result in the same thrust as measured in the bounded flow scenarios. In theory these same blockage correction principles should be useful in adapting V_{OD} for higher blockage ratios and were therefore investigated.

Most blockage correction methods such as those proposed by Mikkelsen and Sorensen (2002) and Barnsley and Wellicome (1990), typically rely on prior knowledge of the bypass flow velocity and flow velocity through the turbine. However, these values are often unknown during the time of analysis. The approach proposed by Werle (2010) provides an adapted C_T for wind turbines based on the blockage ratios. This approach accounts for the confined flow effect on the thrust coefficient. The same theory holds for water flow. Applying this wind turbine blockage correction model to the HK results in this study indicated exaggerated estimations of the results, this was found to agree with previous testing of this model on HK turbines (Ross and Polagye, 2020). However, a correlation trend was prevalent, and through an empirical model adjustment, acceptable correlation to experimental results was observed. The blockage correction formation was adjusted and incorporated into the minimum velocity (V_{OD}) equation as follows:

$$V_{OD} = U_\infty \sqrt{1 - \frac{(1 - \Delta\beta)^2}{1 + \Delta\beta} C_T} \tag{8}$$

Where the $\Delta\beta$ is calculated as follows:

$$\Delta\beta = \beta - 0.07 \tag{9}$$

The V_{OD} equation (8) allows an approximation of this value through only the turbine thrust, swept area and inflow velocity. This indicates a clear relationship between the thrust coefficient and V_{OD}. Seven experimental test cases at low TI's are shown in Fig. 14 where the distribution between V_{OD} values calculated through the V_{OD} approximation and measured from wake results are compared. The results indicate the good approximation of the calculated minimum velocity through to the values measured experimentally. The general trend of higher V_{OD} values for turbines operating at higher thrust coefficients is also indicated by the linear trendline.

The point of V_{OD} occurrence ($X_{\min}$) depends not only on the β and TI, but on the extent of the C_T value. HAHT's with higher C_T's cause a larger disturbance in the flow, resulting in a higher V_{OD}. Within the dataset it was observed that larger disturbance resulted in a faster mixing rate in the near wake due to the larger differential velocity between the wake and bypass flow. Therefore, a general trend was observed, indicating that $X_{\min}$ moved further downstream for cases with lower V_{OD}'s. This relationship only holds true for low TI values. As the TI increased the $X_{\min}$ also moved further upstream.

Previous analyses have concluded with a set point for the efflux velocity, occurring around 1.1 d_t downstream (Lam and Chen, 2014; Whale et al., 1996). Berger et al. (1981) suggested for a ship propeller the position of maximum velocity (R_{mo}) can be predicted as a function of the radius of the propeller (R) and the radius of the propeller hub (R_h):

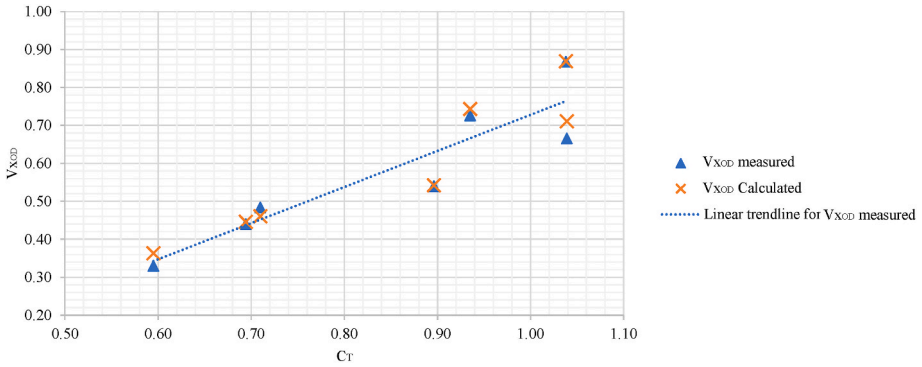

Fig. 14. Relationship between C_T and V_{OD} for the 7 modelled turbines operating at optimal λ.

$$R_{mo} = 0.67(R - R_h) \tag{10}$$

Prosser (1968) proposed a value of 60% of the blade radius from the hub be used. Hamill et al. (2004) proposed rather 0.7 in place of 0.67 shown in the formula by Berger et al. (1981). Lam et al. (2015b) compared empirical equations to experimental results for HAHT's and the equation by Berger et al. (1981) has the closest correlation. Lam et al. (2015b) recommended the equation by Berger et al. (1981) to determine the point of lowest velocity occurrence in the wake of a HAHK device.

In all experiments in the current study the $X_{\min}$ occurred between 1.1 and 1.5 dt downstream. As near wake results are not of primary importance in the current model, the $X_{\min}$ point is chosen to be at a maximum of $1.5d_t$. This significantly simplifies the wake determination and allows simpler incorporation of TI through the dissipation rate. However, it should be noted when determining the $X_{\min}$ in higher V_{OD} cases the position of $X_{\min}$ is generally closer to $d_t = 1$. Where the location of V_{OD} is important, the equation by Berger et al. (1981) should be utilised.

3.5. Dissipation rate

After the initial near wake formation, where the lowest velocity point (V_{OD}) exists, the wake continues to dissipate for a distance downstream. Based on the experimental wake results it was observed that the dissipation rate after V_{OD} is primarily governed by the environmental conditions such as ambient turbulence intensity (TI) and blockage ratio (β), as well as the initial magnitude of the disturbance (magnitude of V_{OD}).

A regression analysis was used to incorporate these parameters of importance into a useable dissipation equation. In literature, linear relationships between V_{OD}/V_∞ and x/D have previously been determined through an experimental dataset (Lam et al., 2015b; Oppong et al., 2020). Although this approach was tested, it did not result in a satisfactory wake prediction. Additionally, large variations in wake behaviour (>20%) were observed when testing the model by Lam et al. (2015a) which is based on a linear approach. In this study a non-linear regression analysis is used instead.

The dissipation rate is determined as a function of the minimum cylindrically averaged velocity deficit in the near wake (Vx_{OD}). The dissipation rate is calculated from a conservative assumed $X_{\min}$ of 1.5 d_t downstream of the hub. The velocity deficit averaged over the turbine swept area (unitless), at various distances downstream (V_x) was determined as:

$$V_x = Vx_{OD} \times C_a \times e^{-Vx_{OD} \times C_b \times dt} \tag{11}$$

where C_a and C_b are coefficients determined through a non-linear regression analysis of the metrics of consideration and d_t is the distance downstream as a function of turbine diameter. The coefficients were determined as:

$$C_a = 1.37 - 0.035 \times TI \tag{12}$$

$$C_b = \left(1.25 \times \beta^{\frac{1}{8}}\right)\left(0.0031 \times TI^2 - 0.033TI + 0.3463\right) \tag{13}$$

The dissipation rate was tested over the following ranges which are representative of installation conditions:

- Turbulence intensities of 5%–20%
- Blockage ratios of 4%–18%.

The maximum differential in velocity deficit in the wake at various distances downstream of the turbine can be seen in Table 5 for a variation of TI values and Table 6 over a range of β's. The modelled values proved to be within 10% of the experimental results past 4 d_t downstream, with very few cases showing slightly higher differences in the V_x approximation in the near wake.

3.6. Model testing

The final model was tested over a range of conditions and turbine types. Due to the large computational requirements per model, a combination of varying operational conditions and turbine geometries were tested to ensure that specifically the turbine thrust, ambient TI and β were included both independently and as a combined effect. As an indication of the model accuracy, the root mean squared error (*rmse*) of the experimental velocity deficit ($V_{x,exp}$) and predicted velocity deficit ($V_{x,model}$) at incremental distance downstream relative to the turbine diameter (d_t), were analysed. The *rmse* for each turbine dataset used as well as the overall *rmse* over all datasets can be seen in Fig. 15.

$$rmse = \sqrt{\frac{\sum_{i=1}^{n}\left(V_{x,exp} - V_{x,model}\right)^2}{n}} \tag{14}$$

As depicted in Fig. 15, the predicted wakes of the 3-bladed (*_3b) and 2-bladed (*_2b) turbines exhibited a strong correlation with the experimental results, accurately capturing the trends in wake dissipation. The largest variations were found in the T3 models (form validation case (Morris, 2014)), which had extremely high turbine thrust measurements resulting in certain variations in the behaviour of the initial near wake. The comparison of the 4-bladed turbines (T3_4b) results showed under prediction of the extent of velocity deficits in the near wake. However, a lack of data on 4-bladed turbines prevented further model calibration. Despite this near wake effect all datasets proved to be within 10% of experimental values past 4 d_t downstream indicating good prediction of the wake behaviour for typical inland conditions.

3.7. Model limitations and considerations

The goal of the semi-empirical model was to provide an approximation of the wake deficit with an accuracy of within 10%. However, it

Table 5
Velocity deficit percentage difference at various TI's at a low blockage ratio.

Ambient Turbulence intensity (TI%)	Percentage difference at a given distance from the turbine hub (%)									
	$d_t = 2$	$d_t = 4$	$d_t = 6$	$d_t = 8$	$d_t = 10$	$d_t = 12$	$d_t = 14$	$d_t = 16$	$d_t = 18$	$d_t = 20$
4–6%	1.9	4.3	4.4	3.1	1.9	1.0	0.9	1.7	2.5	0.1
9–11%	5.9	2.3	1.4	1.2	1.0	0.7	0.4	0.2	0.2	0.1
16–18%	2.9	0.9	1.1	1.2	1.0	0.7	0.3	0.2	0.1	0.1
Maximum differential in dataset	**8.1**	**9.3**	**8.7**	**5.4**	**2.5**	**1.4**	**1.4**	**1.6**	**2.5**	**0.1**

Table 6
Velocity deficit percentage difference at various blockage ratios (measured over a range of TI's).

Blockage ratio β (%)	Percentage difference at a given distance from the turbine hub (%)									
	$d_t = 2$	$d_t = 4$	$d_t = 6$	$d_t = 8$	$d_t = 10$	$d_t = 12$	$d_t = 14$	$d_t = 16$	$d_t = 18$	$d_t = 20$
<7%	3.3	2.8	2.6	2.0	1.4	0.8	0.6	0.5	0.6	0.1
13%	0.5	0.1	0.4	0.9	1.4	0.7	0.5	0.1	0.1	0.1
17%	4.8	3.0	1.9	1.7	1.6	1.4	1.1	0.7	0.3	0.1
Maximum differential in dataset	**12.6**	**6.0**	**2.5**	**3.1**	**3.1**	**2.8**	**2.5**	**1.9**	**0.6**	**0.1**

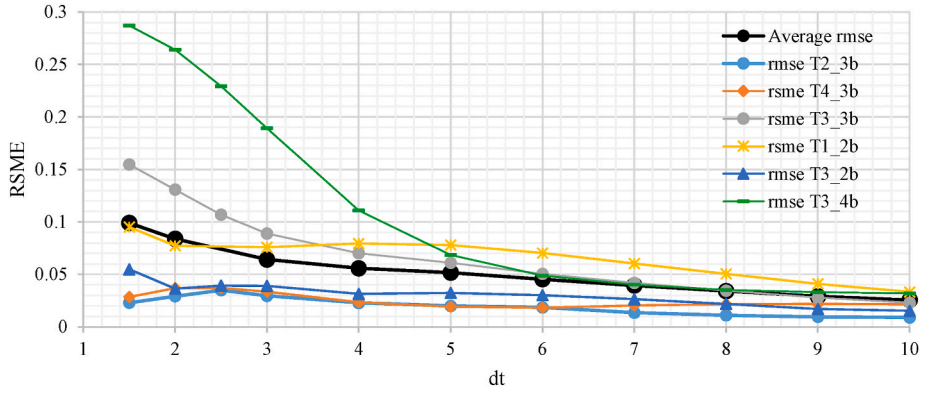

Fig. 15. Wake model prediction error over a range of test conditions.

is important to consider several limitations due to the nature of the model development, simplification of wake metric effect, and the use of RANS-CFD for generating the experimental data. Some specific limitations to be noted include:

- Wake results from laboratory tests were used for the benchmark validation of the CFD models, however, few of these laboratory tests have wake results exceeding 10 d_t downstream of the turbine. Model behaviour after this point appears to be a reasonable approximation, but a consideration of possible inaccuracies in the far wake is necessary. It is assumed that any inaccuracies in the model would be attributed to slower dissipation, as a result of the absence of high turbulence values in the bypass flow within the far wake. Consequently, the model is anticipated to yield conservative predictions.
- Additional environmental and operational effects such as drastic differences in turbine geometry (e.g., blade numbers) may alter wake formation. However, the model was developed in a way that allows further calibration and inclusion of any further parameters affecting the wake development. The current model was not tested over a wide range of turbine solidities and most turbine tests were 3-bladed (as these are currently most efficient and most produced).
- As the model was developed for simplistic application in the preliminary design or site assessment stages where minimal turbine details are known, it is expected that some inaccuracies may result from the oversimplification of the model. This should be considered where exact wake propagation is relevant (e.g., for possible scour or sedimentation analysis or where spacing is a limited parameter). More complex and detailed wake models should be used when more details are available on the specific turbine planned for installation, especially as wake width is not considered here.
- The model was built with the assumption that sufficient submergence depths have been ensured. In cases where the turbine is near to the free surface the water surface boundary may affect wake propagation.
- For array schemes the inter-effect of coinciding wakes was not included. Variations of these effects have been investigated in the past and could be referred to (Nuernberg and Tao, 2018; Gajardo et al., 2019).

Previous HK wake models have typically overlooked the impact of blockage ratio, and only a limited number of studies have included two or three variations of TI's. The current model provides a significant improvement to existing HAHT analytical wake models by incorporating these important factors. Through including multiple turbine types and operational conditions it was possible to ascertain the model applicability over a range of results.

3.8. Typical HAHT wake in inland flow

A prediction of wake dissipation in canal systems based on the developed semi-empirical model can be seen in Figs. 16 and 17. Fig. 16 specifically indicates the effect of C_T and TI where Fig. 17 depicts wake propagation over the variation of TI and β for a turbine operating at optimal λ and at a relatively high C_p (high efficiency). The plots depict a range of TI's between 5 to 20%, which is commonly observed in canal systems. These plots can serve as a visual reference guide on typical

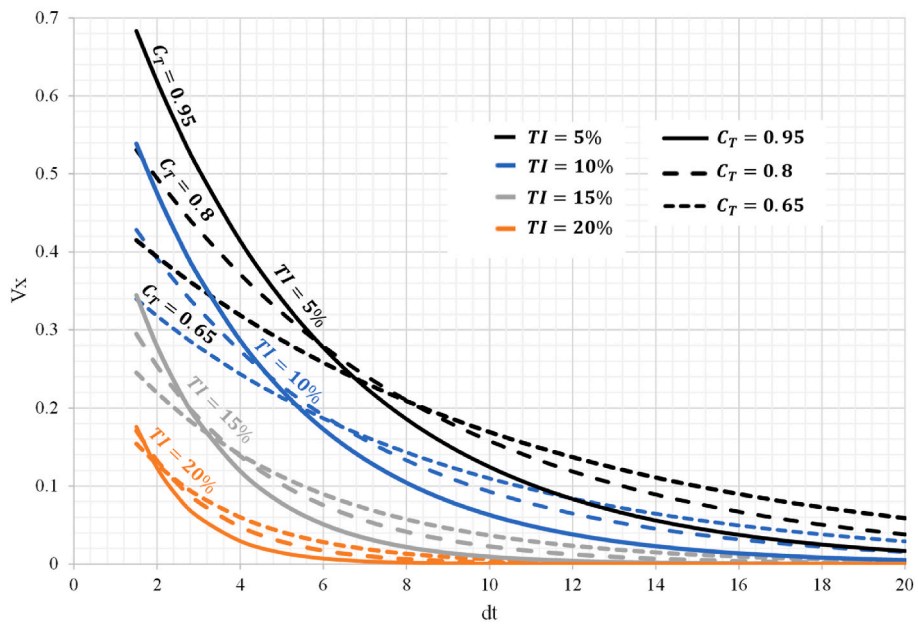

Fig. 16. Typical wake dissipation for varying C_T and turbulence intensities (TI) for a 3-bladed turbine.

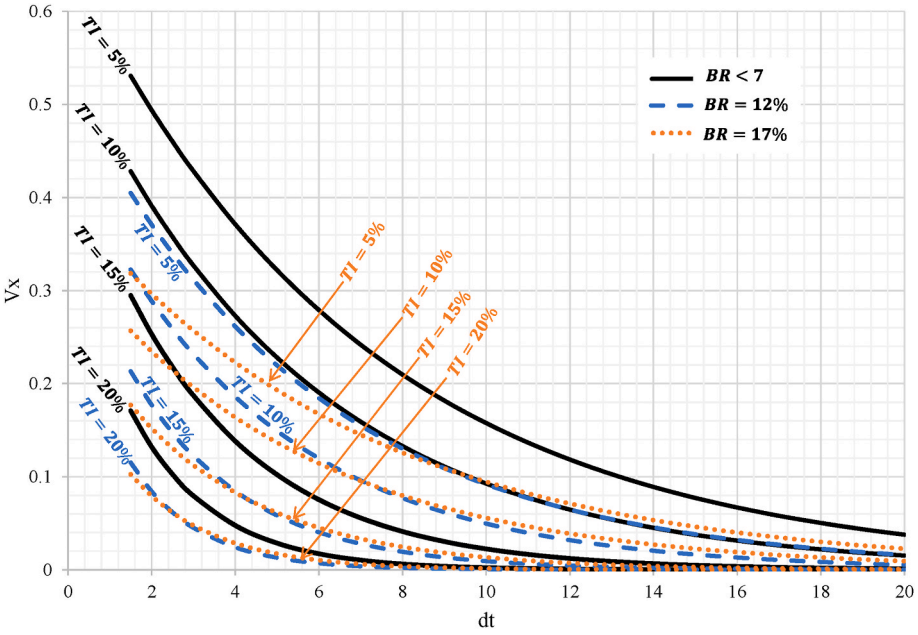

Fig. 17. Typical wake dissipation for varying Blockage ratios and turbulence intensities (TI) at a typical C_T of 0.8 for a 3-bladed turbine.

wake behaviour.

4. Conclusions

A semi-empirical calculation method for the decay of a single hydrokinetic turbine wake is formulated for uniform unbounded flow, and then adjusted for bounded flow and changes in turbulence changes. The mean momentum integral, which demonstrates the momentum deficit in the wake, can be estimated through the thrust of the turbine. Previous models have concluded this may be exclusively determined through thrust; however, the current experimental results show blockage ratio and TI should also be considered. A semi-empirical relationship for the wake dissipation rate in the near and far wake is determined through theoretical relationships and experimental data from various validated CFD models.

The findings and consequently developed model allow a description of the wake characteristics and assist in estimating the wake dissipation with the minimum required information. It also assists in providing an overview of wake changes for important parameters of consideration (referred to here as wake change metrics) which are primarily the turbine thrust at operating point (C_T), the ambient turbulence intensity of the flow (TI) and the blockage ratio, being the ratio of turbine swept area over the channel flow area. The following summarizes these primary effects on the wake dissipation:

- Higher C_T results in a higher efflux velocity and thus higher disturbance in the flow field.

- Higher TI values result in faster wake dissipation and thus also cause the X_{min} (point of minimum velocity) to move further upstream in the wake.
- Higher blockage ratios lead to faster wake dissipation overall, as there is limited space for the bypass flow to decelerate. Consequently, the wake dissipation process is accelerated. Although this effect may vary depending on channel shapes and width to height ratios, the overall effect of wall distance is included in the semi-empirical model.

This wake model solution is a simplified approach to predicting the extreme complexities in the flow field downstream of a HK device. It however allows an overview of the general wake behaviour and limits over estimation of wake lengths leading to long distances required between turbines in inland array designs. Additionally, the proposed model limits the application complexities, making it useful as a reference guide. It also includes typical flow conditions experienced in channels with favourable installation conditions for inland HAHT devices.

Declaration of competing interest

The authors declare the following financial interests/personal relationships which may be considered as potential competing interests: Chantel Niebuhr reports equipment, drugs, or supplies was provided by University of Pretoria. Chantel niebuhr reports equipment, drugs, or supplies was provided by Center for high performance computing cape town.

Data availability

Data will be made available on request.

Acknowledgements

This work was supported by the University of Pretoria. The computational capabilities were made possible due to academic hours allocated by the Center for High-Performance Computing (CHPC) South Africa. Siemens STAR-CCM + Simcenter software and support were provided by Aerotherm Computational Dynamics (Pty) Ltd. Experimental results were obtained from the Sandia Laboratories repository as well as other referenced literature. All contributors are thanked for their kind assistance and support.

References

Ahmadi, M.H.B., 2019. Influence of upstream turbulence on the wake characteristics of a tidal stream turbine. Renew. Energy 132, 989–997.
Bachant, P., Wosnik, M., 2016. Effects of Reynolds number on the energy conversion and near-wake dynamics of a high solidity vertical-Axis cross-flow turbine. Energies. https://doi.org/10.3390/en9020073.
Bahaj, A.S., Wmjj, Batten, McCann, G., 2007. Experimental verifications of numerical predictions for the hydrodynamic performance of horizontal axis marine current turbines. Renew. Energy 32, 2479–2490.
Barnsley, M.J., Wellicome, J.F., 1990. Final Report on the 2nd Phase of Developmeent and Testing of a Horizontal axis Wind Turbine Rig for the Investigation of Stall Regulation Aerodynamics.
Berger, W., FelKel, K., Hager, M., Oebius, H., Schale, E., 1981. Courant provoque par les bateaux protection des berges et solution pour eviter l'erosion du lit du haut rhin. PIANC, 25th Congr.
Birjandi, A.H., Woods, J., Bibeau, E.L., 2012. Investigation of macro-turbulent flow structures interaction with a vertical hydrokinetic river turbine. Renew. Energy 48, 183–192.
Blackmore, T., Batten, W.M.J., Bahaj, A.S., 2014. Influence of turbulence on the wake of a marine current turbine simulator. Proc R Soc A Math Phys Eng Sci 470, 1–17.
Cardona-Mancilla, C., Rio, J.S., Hincapié-zuluaga, D., Chica, E., 2018. A numerical simulation of horizontal Axis hydrokinetic turbine with and without augmented diffuser. Int. J. Renew. Energy Resour. 8.
Chawdhary, S., Hill, C., Yang, X., Guala, M., Corren, D., Colby, J., Sotiropoulos, F., 2017. Wake characteristics of a TriFrame of axial-flow hydrokinetic turbines. Renew. Energy 109, 332–345.
Churchfield, M.J., Li, Y., Moriarty, P.J., 2013. A large eddy simulation study of wake propagation and power production in an array of tidal-current turbines. Philos Trans R Soc A 371, 1–15.
Consul, C.A., Willden, R.H.J., McIntosh, S.C., 2013a. Blockage effects on the hydrodynamic performance of a marine cross-flow turbine. Philos Trans R Soc A Math Phys Eng Sci. https://doi.org/10.1098/rsta.2012.0299.
Consul, C.A., Willden, R.H.J., McIntosh, S.C., 2013b. Blockage effects on the hydrodynamic performance of a marine cross-flow turbine. Philos Trans R Soc A. https://doi.org/10.1098/rsta.2012.0299.
Eggleston, D.M., Stoddard, F., 1987. Wind Turbine Engineering Design. Van Nostrand Reinhold Company Inc., New York.
El Fajri, O., Bhushan, S., Thompson, D.S., O'Doherty, T., 2020. Numerical investigation of shallow-water effects on hydrokinetic turbine wake recovery. Int Mar Energy J 3, 25–35.
El Fajri, O., Bowman, J., Bhushan, S., Thompson, D., O'Doherty, T., 2022. Numerical study of the effect of tip-speed ratio on hydrokinetic turbine wake recovery. Renew. Energy 182, 725–750.
Frandsen, S., Barthelmie, R., Pryor, S., Rathmann, O., Larsen, S., 2006. Analytical modelling of wind speed deficit in large offshore wind farms. Wind Energy 9, 39–53.
Gajardo, D., Escauriaza, C., Ingram, D.M., 2019. Capturing the development and interactions of wakes in tidal turbine arrays using a coupled BEM-DES model. Ocean Eng. 181, 71–88.
Garrett, C., Cummins, P., 2007. The efficiency of a turbine in a tidal channel. J. Fluid Mech. 588, 243–251.
Ge, M., Wu, Y., Liu, Y., Yang, X.I.A., 2019. A two-dimensional Jensen model with a Gaussian-shaped velocity deficit. Renew. Energy 141, 46–56.
Glauert, H., 1983. The elements of aerofoil and airscrew theory. https://doi.org/10.1017/CBO9780511574481.
Gotelli, C., Musa, M., Guala, M., Escauriaza, C., 2019. Experimental and numerical investigation of wake interactions of marine hydrokinetic turbines. Energies 12, 1–17.
Guerra, M., Thomson, J., 2019. Wake measurements from a hydrokinetic river turbine. Renew. Energy 139, 483–495.
Hamill, G.A., McGarvey, J.A., Hughes, D.A.B., 2004. Determination of the efflex velocity from a ship's propeller. Proc Inst Civ Eng Marit Eng 157, 83–91.
Harrison, M.E., Batten, W.M.J., Myers, L.E., Bahaj, A.S., 2010. Comparison between CFD simulations and experiments for predicting the far wake of horizontal axis tidal turbines. IET Renew. Power Gener. 4, 613.
Hill, C., Neary, V.S., 2014. U. S. Department of energy reference model program RM1 : experimental results. Sandia Natl. Lab.
Hill, C., Neary, V.S., Gunawan, B., Guala, M., Sotiropoulos, F., 2014. U. S. Department of Energy Reference Model Program RM1 : Experimental Results (Minneapolis).
Hill, C., Neary, V.S., Guala, M., Sotiropoulos, F., 2020. Performance and wake characterization of a model hydrokinetic turbine: the reference model 1 (RM1) dual rotor tidal energy converter. In: Energies, pp. 1–21.
Houlsby, G., Vogel, C., 2017. In: Civ, Proc Inst, Water, Eng (Eds.), The Power Available to Tidal Turbines in an Open Channel Flow. Marit. Energy, pp. 12–21.
Jensen, N.O., 1983. A note on wind generator interaction. Risø-M-2411 Risø Natl Lab Roskilde 1–16.
Kinsey, T., Dumas, G., 2017. Impact of channel blockage on the performance of axial and cross- flow hydrokinetic turbines. Renew. Energy 103, 239–254.
Koh, W.X.M., Ng, E.Y.K., 2017. A CFD Study on the Performance of a Tidal Turbine under Various Fl Ow and Blockage Conditions, 107, pp. 124–137.
Kolekar, N., Banerjee, A., 2015. Performance characterization and placement of a marine hydrokinetic turbine in a tidal channel under boundary proximity and blockage effects. Appl. Energy 148, 121–133.
Kolekar, N., Hu, Z., Banerjee, A., Du, X., 2013. Hydrodynamic design and optimization of hydro - kinetic turbines using a robust design method. In: Proc. 1st Mar. Energy Technol. Symp, pp. 1–10.
Lam, W.H., Chen, L., 2014. Equations used to predict the velocity distribution within a wake from a horizontal-axis tidal-current turbine. Ocean Eng. 79, 35–42.
Lam, W., Hamil, G.A., Song, Y.C., Robinson, D.J., Raghunathan, S., 2011. A review of the equations used to predict the velocity distribution within a ship's propeller jet. Ocean Eng. 38, 1–10.
Lam, W., Chen, L., Hashim, R., 2015a. Analytical Wake Model of Tidal Current Turbine, 79, pp. 512–521.
Lam, W.H., Chen, L., Hashim, R., 2015b. Analytical wake model of tidal current turbine. Energy 79, 512–521.
Larsen, G.C., 1988. A Simple Wake Calculation Procedure, 2760. Risø-M No, p. 58.
Li, Y., Colby, J.A., Kelley, N., Thresher, R., Jonkman, B., Hughes, S., 2010. Inflow measurements in a tidal strait for deploying tial current turbines: lessons, opportunities and challenges. Proc. 29th Int. Conf. Ocean. Offshore Artic Eng.
Lloyd, T.P., Turnock, S.R., Humphrey, V.F., 2014. Assessing the influence of inflow turbulence on noise and performance of a tidal turbine using large eddy simulations. Renew. Energy 71, 742–754.
Lo Brutto, O.A., Nguyen, V.T., Guillou, S.S., Gualous, H., Boudart, B., 2015. Reanalyse of an analytical model for one tidal turbine wake prediction. Proc. 11th Eur. Wave Tidal Energy Conf.
Ma, Y., Lam, W.H., Cui, Y., Zhang, T., Jiang, J., Sun, C., Guo, J., Wang, S., Lam, S.S., Hamill, G., 2018. Theoretical vertical-axis tidal-current-turbine wake model using axial momentum theory with CFD corrections. Appl. Ocean Res. 79, 113–122.
Macleod, A.J., Barnes, S., Rados, K.G., Bryden, I.G., 2002. Wake effects in tidal current turbine farms. MAREC 2002.
Maganga, F., Germain, G., King, J., Pinon, G., Rivoalen, E., 2010. Experimental characterisation of flow effects on marine current turbine behaviour and on its wake properties. IET Renew. Power Gener. 4, 498–509.

Mikkelsen, R., Sorensen, J.N., 2002. Modelling of wind tunnel blockage. Glob. Wind. Conf.
Milne, I.A., Sharma, R.N., Flay, R.G.J., Bickerton, S., 2013. Characteristics of the turbulence in the flow at a tidal stream power site. Philos Trans R Soc A Math Phys Eng Sci. https://doi.org/10.1098/rsta.2012.0196.
Morris, C., 2014. Influence of Solidity on the Performance, Swirl Characteristics, Wake Recovery and Blade Deflection of a Horizontal Axis Tidal Turbine.
Morris, C.E., O'Doherty, D.M., Mason-Jones, A., O'Doherty, T., 2016. Evaluation of the swirl characteristics of a tidal stream turbine wake. Int J Mar Energy 14, 198–214.
Mourad, M.G., Ayad, S.S., Abdellatif, O.E., Abdelaziz, A.A., 2015. An experimental study of the near wake of horizontal axis wind turbines. 13th Int Energy Convers Eng Conf. https://doi.org/10.2514/6.2015-3714.
Mycek, P., Gaurier, B., Germain, G., Pinon, G., Rivoalen, E., 2014. Experimental study of the turbulence intensity effects on marine current turbines behaviour. Part II: two interacting turbines. Renew. Energy 68, 876–892.
Myers, L., Bahaj, A.S., 2007. Wake studies of a 1/30th scale horizontal axis marine current turbine. Ocean Eng. 34, 758–762.
Niebuhr, C.M., van Dijk, M., Bhagwan, J.N., 2019. Development of a design and implementation process for the integration of hydrokinetic devices into existing infrastructure in South Africa. WaterSA 45, 434–446.
Niebuhr, C.M., Schmidt, S., van Dijk, M., Smith, L., Neary, V.S., 2022. A review of commercial numerical modelling approaches for axial hydrokinetic turbine wake analysis in channel flow. Renew. Sustain. Energy Rev. 158, 112151.
Nishino, T., Willden, R.H.J., 2012. Effects of 3-D channel blockage and turbulent wake mixing on the limit of power extraction by tidal turbines. Int. J. Heat Fluid Flow 37, 123–135.
Nuernberg, M., Tao, L., 2018. Experimental study of wake characteristics in tidal turbine arrays. Renew. Energy 127, 168–181.
Olczak, A., Stallard, T., Feng, T., Stansby, P.K., 2016. Comparison of a RANS blade element model for tidal turbine arrays with laboratory scale measurements of wake velocity and rotor thrust. J. Fluid Struct. 64, 87–106.
Oppong, S., Haur, W., Guo, J., et al., 2020. Predictions of wake and central mixing region of double horizontal Axis tidal turbine. KSCE J. Civ. Eng. 24, 1983–1995.
Palm, M., Huijsmans, R., Pourquie, M., Sijtstra, A., 2010. Simple wake models for tidal turbines in farm arrangement. In: ASME 2010 29th Int. Conf. Ocean. Offshore Arct. Eng. Am. Soc. Mech. Eng., pp. 577–587.
Palm, M., Huijsmans, R., Pourquie, M., Sijtstra, A., 2011. The applicability of semiempirical wake models for tidal farms. Proc. 9th Eur. Wave Tidal Energy Conf.
Prosser, M.J., 1968. Propeller Induced Scour.
Pyakurel, P., Vanzwieten, J.H., Wenlong, T., Ananthakrishnan, P., 2017a. Analytic characterization of the wake behind in-stream hydrokinetic turbines. Mar. Technol. Soc. J. 51, 58–71.
Pyakurel, P., Vanzwieten, J.H., Dhanak, M., Xiros, N.I., 2017b. Numerical modeling of turbulence and its effect on ocean current turbines. Int J Mar Energy 17, 84–97.
Pyakurel, P., Tian, W., VanZwieten, J.H., Dhanak, M., 2017c. Characterization of the mean flow field in the far wake region behind ocean current turbines. J Ocean Eng Mar Energy 3, 113–123.
Ross, H., Polagye, B., 2020. An experimental assessment of analytical blockage corrections for turbines. Renew. Energy 152, 1328–1341.
Sanderse, B., van der Pijl, S.P., Koren, B., 2011. Review of computational fluid dynamics for wind turbine wake aerodynamics. Wind Energy 14, 799–819.
Shen, W.Z., Mikkelsen, R., Sorensen, J.N., 2005. Tip loss corrections for wind turbine Computations. Wind Energy 8, 457–475.
Siddiqui, M.S., Rasheed, A. di, Kvamsdal, T., Tabib, M., 2017. Influence of tip speed ratio on wake flow characteristics utilizing fully resolved CFD methodology. J Phys Conf Ser. https://doi.org/10.1088/1742-6596/854/1/012043.
Silva, P.A.S.F., De Oliveira, T.F., Brasil Junior, A.C.P., Vaz, J.R.P.P., Oliveira, T.F.D.E., Junior, A.C.P.B., Vaz, J.R.P.P., 2016. Numerical study of wake characteristics in a horizontal-Axis hydrokinetic turbine. Ann Braziian Acad Sci 88, 2441–2456.
Stallard, T., Collings, R., Feng, T., Whelan, J., 2013. Interactions between tidal turbine wakes: experimental study of a group of three-bladed rotors. Philos Trans R Soc A Math Phys Eng Sci. https://doi.org/10.1098/rsta.2012.0159.
Stewart, D.P.J., 1992. Characteristics of a Ship's Screw Wash and the Influence of Quay Wall Proximity. Queen's University of Belfast.
Tedds, S.C., Owen, I., Poole, R.J., 2014. Near-wake characteristics of a model horizontal axis tidal stream turbine. Renew. Energy 63, 222–235.
Tian, W., Mao, Z., Ding, H., 2018. Design, test and numerical simulation of a low-speed horizontal axis hydrokinetic turbine. Int. J. Nav. Archit. Ocean Eng. 10, 782–793.
Wang, S., Lam, W.H., Cui, Y., Zhang, T., Jiang, J., Sun, C., Guo, J., Ma, Y., Hamill, G., 2018. Novel energy coefficient used to predict efflux velocity of tidal current turbine. Energy 158, 730–745.
Werle, M.J., 2010. Wind turbine wall-blockage performance corrections. J. Propul. Power 26, 1317–1321.
Whale, J., Papadopoulos, K.H., Anderson, C.G., Skyner, D.J., Helmis, C.G., 1996. A study of the near wake structure of a wind turbine comparing measurements from laboratory and full-scale experiments. Sol. Energy 56, 621–633.
Whelan, J.I., Graham, J.M.R.R., Peiro, J., Peiró, J., 2009. A free-surface and blockage correction for tidal turbines. J. Fluid Mech. 624, 281–291.
Williams, G., Jain, P., 2011. Renewable energy strategies. Sustain a J Environ Sustain issues 29–42.
Zhang, Y., Zhang, J., Lin, X., Wang, R., Zhang, C., Zhao, J., 2020. Experimental investigation into downstream field of a horizontal axis tidal stream turbine supported by a mono pile. Appl. Ocean Res. 101, 102257.